Anal. Chem. **2010,** *82,* 5189–5194

"Seeing and Counting" Individual Antigens Captured on a Microarrayed Spot with Force-Based Atomic Force Microscopy

Dhruvajyoti Roy, Sung Hong Kwon, Ju-Won Kwak, and Joon Won Park*

Department of Chemistry, National Core Research Center for Systems Bio-Dynamics, Pohang University of Science and Technology (POSTECH), Pohang 790-784, Korea

The mapping capability of atomic force microscopy (AFM) enabled us to see captured prostate-specific antigens (PSAs) on a spot microarrayed with the corresponding antibody and count the number of the antigens in a submicrometer area. To enhance the reliability and the reproducibility of the approach, a third-generation dendron was employed for the surface treatment. The specific force between the captured PSA and the detection antibody (5A6) was measured after cross-linking, and the mean unbinding force was 56 ± 2 pN. At 100 fM, there were 12 captured antigens in 4.32×10^4 nm^2, and the number was dependent upon the concentration. A larger hydrodynamic distance (8 ± 2 nm) of the immunocomplex resulted in a cluster of pixels corresponding to the single complex in a map recorded over a selected area with a positional interval of 3 nm, and this feature helped to discriminate between pixels of the specific interaction and the nonspecific ones. The results indicate that the approach can be applicable to the quantitative analysis of the antigen in a sample and imply that it can be extended to a sample of very low copy numbers as long as the size of the microarrayed spot is reduced.

The specific molecular recognition in biological systems plays a key role in regulating many biological processes in nature. The specificity is governed by multiple noncovalent bonds (e.g., electrostatic, van der Waals, and hydrogen) and hydrophobic interactions. Among the various ligand−receptor interactions, the antigen−antibody interaction has great fundamental and practical relevance. The antigen−antibody interactions are widely analyzed by the conventional enzyme-linked immunosorbent assay (ELISA);[1] however, the sensitivity and resolution of ELISA is rather limited, and a persistent challenge in this area is the lack of highly sensitive readout technologies. The interest in the detection of antigens at ultralow levels is substantial because numerous protein markers for cancers, infectious diseases, and biochemical processes are present at very low concentrations in certain circumstances, and a highly sensitive detection approach can be useful for analyzing proteins from a few cells or even a single cell.

The microarray-based platform is of great interest for analyzing protein interactions because of its nature of high-throughput and easy integration with microfluidic devices.[2] Typically, the microarray assay employs fluorescence detection,[3] and a number of interesting detection techniques (e.g., optical,[4] amperometric,[5] radiochemical,[6] and mass spectroscopy[7]) have been explored to increase the sensitivity and the detection limit. For example, in searching for sensitive and specific methods for protein biomarker detection, the Mirkin group reported a nanoparticle-based biobarcode assay technology for substantial amplification in prostate-specific antigen (PSA) detection.[8] Recently, Lee et al. reported a new signal amplification strategy for mass spectrometry by using small-molecule-tagged gold microparticles for target proteins, such as adiponectin and α-fetoprotein.[9]

In recent years, considerable advancement of the scanning probe microscopes has offered a variety of experimental tools for label-free detection of biomarkers. In particular, the nanomechanical cantilever sensors have been successfully used for biomolecular detection based on the bending-plate principle.[10] This technology has been used for detecting biomarkers, such as PSA,[11] and cardiac biomarker proteins[12] at clinically relevant conditions and concentrations. In contrast, the atomic force microscope (AFM) using a conventional probe (a cantilever with an integrated sharp tip at its terminus) has become well-established as a crucial tool in diverse fields, in particular, in the biological sciences due to its capability of operating in a fluid environment.[13−15] A rational

* To whom correspondence should be addressed. E-mail: jwpark@postech.ac.kr.

(1) Crowther, J. R. *The ELISA Guidebook*; Humana Press: Totowa, NJ, 2000.
(2) Haab, B. B. *Curr. Opin. Biotechnol.* **2006**, *17*, 415–421.
(3) Gu, Q.; Sivanandam, T. M.; Kim, C. A. *Proteome Sci.* **2006**, *4*, 21.
(4) Willumsen, B.; Christian, G. D.; Rozicka, J. *Anal. Chem.* **1997**, *69*, 3482–3489.
(5) Duan, C.; Meyerhoff, M. E. *Anal. Chem.* **1994**, *66*, 1369–1377.
(6) Chard, T. *An Introduction to Radioimmunoassay and Related Techniques*; Elsevier: Amsterdam, 1987.
(7) Gaspari, M.; Cheng, M. M.-C.; Terracciano, R.; Liu, X.; Nijdam, A. J.; Vaccari, L.; di Fabrizio, E.; Petricoin, E. F.; Liotta, L. A.; Cuda, G.; Venuta, S.; Ferrari, M. *J. Proteome Res.* **2006**, *5*, 1261–1266.
(8) Nam, J.-M.; Thaxton, C. S.; Mirkin, C. A. *Science* **2003**, *301*, 1884–1886.
(9) Lee, J. R.; Lee, J.; Kim, S. K.; Kim, K. P.; Park, H. S.; Yeo, W.-S. *Angew. Chem., Int. Ed.* **2008**, *47*, 9518–9521.
(10) Fritz, J.; Baller, M. K.; Lang, H. P.; Rothuizen, H.; Vettiger, P.; Meyer, E.; Güntherodt, H.-J.; Gerber, Ch.; Gimzewski, J. K. *Science* **2000**, *288*, 316–318.
(11) Wu, G.; Datar, R. H.; Hansen, K. M.; Thundat, T.; Cote, R. J.; Majumdar, A. *Nat. Biotechnol.* **2001**, *19*, 856–860.
(12) Arntz, Y.; Seelig, J. D.; Lang, H. P.; Zhang, J.; Hunziker, P.; Ramseyer, J. P.; Meyer, E.; Hegner, M.; Gerber, Ch. *Nanotechnology* **2003**, *14*, 86–90.
(13) Drake, B.; Prater, C. B.; Weisenhorn, A. L.; Gould, S. A. C.; Albrecht, T. R.; Quate, C. F.; Cannell, D. S.; Hansma, H. G.; Hansma, P. K. *Science* **1989**, *243*, 1586–1589.

10.1021/ac100476b
Published on Web 05/14/2010

design of bioanalytical assays requires profound knowledge of biomolecular interactions, and many of those interactions are within the range that AFM can access.[16−18] In this context, direct quantification of biomolecular interactions at the single molecule level by force spectroscopy has emerged as a powerful approach. It can resolve single molecular interaction forces between ligand−receptor pairs,[19−21] complementary DNA nucleotides,[22−24] enzyme−substrate complexes,[25,26] and antigen−antibody complexes.[27−29] This mode of AFM has been widely exploited for mapping binding sites on various surfaces, including living bacteria,[30] red blood cells,[31] bone cells,[32] and endothelial cells,[33] and has even efficiently been used for adhesion mapping on patterned dual-component protein films by using functionalized probes.[34] To retrieve additional information, topographic imaging has been frequently employed in parallel.[35−37] Recently, simultaneous topographic and recognition (TREC) imaging was introduced by Hinterdorfer's group.[38] The approach has been effectively used for single molecule topography and recognition imaging of ligands/receptors,[39,40] planar protein lattices,[41] cells,[42] and membranes.[43] To our knowledge, force-based AFM has not been applied for the analysis of the microarray, and its success will open a new avenue to an intriguing way of analyzing low levels of biomarkers.

In this account, we examined force-based AFM as a tool for analyzing captured antigens on a microarray. Overall, this approach combines two key features: specificity determined by a probe antibody on the microarray format and a label-free AFM readout. The mapping capability of AFM enabled us to see the captured antigens and count them in a submicrometer-designated area. Appropriately controlling the immobilization of a probe molecule on the AFM tip is critical because a less controlled immobilization may result in poor target molecule recognition and a high chance of getting complicated force−distance curves and nonspecific tip−surface interaction.[44,45] To enhance the reliability and reproducibility of this approach, we used a third-generation dendron (27-acid dendron, Supporting Information S1) for the surface treatment. Our previous studies with the dendron-modified AFM tip as well as substrate demonstrated that the treatment results in force−distance curves with mostly a single rupture peak and sharp force histograms, thereby enhancing the capability to discriminate nonspecific bindings.[46−48] For enhanced freedom of movement and better durability, we used a flexible linker to conjugate covalently the detection antibody at the apex of the immobilized 27-acid dendron on the tip surface.

For this study, we have chosen PSA, which is the well-studied prostate cancer biomarker. It is a 33 kDa glycoprotein that belongs to the kallikrein family,[49] is produced in prostate tissues, and is secreted into seminal fluid.[50] For post-operative patients, PSA concentration in serum becomes very low, and monitoring the copy number would be beneficial for the prognosis. PSA may also be a good biomarker for breast cancer,[51] but the low level of PSA in women avoids convenient detection. In this context, a new capability of the force-based AFM is demonstrated by utilizing two distinct monoclonal antibodies specific to two different epitopes of PSA.

MATERIALS AND METHODS

General. Dendron-modified glass slides were purchased from NSB Postech Inc. (www.nsbpostech.com). The dendron that was used for the tip modification, 9-anthrylmethyl-3-({[tris({[(1-{tris[(2-

(14) Bustamante, C.; Rivetti, C.; Keller, D. J. *Curr. Opin. Struct. Biol.* **1997**, *7*, 709–716.
(15) Engel, A.; Muller, D. J. *Nat. Struct. Biol.* **2000**, *7*, 715–718.
(16) Lee, C.-K.; Wang, Y.-M.; Huang, L.-S.; Lin, S. *Micron* **2007**, *38*, 446–461.
(17) Rief, M.; Gautel, M.; Oesterhelt, F.; Fernandez, J. M.; Gaub, H. E. *Science* **1997**, *276*, 1109–1112.
(18) Clausen-Schaumann, H.; Seitz, M.; Krautbauer, R.; Gaub, H. E. *Curr. Opin. Chem. Biol.* **2000**, *4*, 524–530.
(19) Florin, E.-L.; Moy, V. T.; Gaub, H. E. *Science* **1994**, *264*, 415–417.
(20) Fritz, J.; Katopodis, A. G.; Kolbinger, F.; Anselmetti, D. *Proc. Natl. Acad. Sci. U.S.A.* **1998**, *95*, 12283–12288.
(21) Moy, V. T.; Florin, E.-L.; Gaub, H. E. *Science* **1994**, *266*, 257–259.
(22) Rief, M.; Clausen-Schaumann, H.; Gaub, H. E. *Nat. Struct. Biol.* **1999**, *6*, 346–349.
(23) Strunz, T.; Oroszlan, K.; Schäefer, R.; Güentherodt, H.-J. *Proc. Natl. Acad. Sci. U.S.A.* **1999**, *96*, 11277–11282.
(24) Lee, G. U.; Chrisey, L. A.; Colton, R. J. *Science* **1994**, *266*, 771–773.
(25) Zhang, Y.; Zhao, D.; Bai, C.; Wang, C. *Life Sciences* **1999**, *65*, PL253–PL260.
(26) Fiorini, M.; McKendry, R.; Cooper, M. A.; Rayment, T.; Abell, C. *Biophys. J.* **2001**, *80*, 2471–2476.
(27) Hinterdorfer, P.; Baumgartner, W.; Gruber, H. J.; Schilcher, K.; Schindler, H. *Proc. Natl. Acad. Sci. U.S.A.* **1996**, *93*, 3477–3481.
(28) Allen, S.; Chen, X.; Davies, J.; Davies, M. C.; Dawkes, A. C.; Edwards, J. C.; Roberts, C. J.; Sefton, J.; Tendler, S. J. B.; Williams, P. M. *Biochemistry* **1997**, *36*, 7457–7463.
(29) Kienberger, F.; Kada, G.; Mueller, H.; Hinterdorfer, P. *J. Mol. Biol.* **2005**, *347*, 597–606.
(30) Dupres, V.; Menozzi, F. D.; Locht, C.; Clare, B. H.; Abbott, N. L.; Cuenot, S.; Bompard, C.; Raze, D.; Dufrêne, Y. F. *Nat. Methods* **2005**, *2*, 515–520.
(31) Grandbois, M.; Dettmann, W.; Benoit, M.; Gaub, H. E. *J. Histochem. Cytochem.* **2000**, *48*, 719–724.
(32) Lehenkari, P. P.; Charras, G. T.; Nykänen, A.; Horton, M. A. *Ultramicroscopy* **2000**, *82*, 289–295.
(33) Almqvist, N.; Bhatia, R.; Primbs, G.; Desai, N.; Banerjee, S.; Lal, R. *Biophys. J.* **2004**, *86*, 1753–1762.
(34) Agnihotri, A.; Siedlecki, C. A. *Ultramicroscopy* **2005**, *102*, 257–268.
(35) Jones, V. W.; Kenseth, J. R.; Porter, M. D.; Mosher, C. L.; Henderson, E. *Anal. Chem.* **1998**, *70*, 1233–1241.
(36) Perrin, A.; Lanet, V.; Theretz, A. *Langmuir* **1997**, *13*, 2557–2563.
(37) Ouerghi, O.; Touhami, A.; Othmane, A.; Ouada, H. B.; Martelet, C.; Fretigny, C.; Jaffrezic-Renault, N. *Sens. Actuators, B* **2002**, *84*, 167–175.
(38) Stroh, C. M.; Ebner, A.; Geretschläger, M.; Freudenthaler, G.; Kienberger, F.; Kamruzzahan, A. S. M.; Smith-Gill, S. J.; Gruber, H. J.; Hinterdorfer, P. *Biophys. J.* **2004**, *87*, 1981–1990.
(39) Ebner, A.; Kienberger, F.; Kada, G.; Stroh, C. M.; Geretschläger, M.; Kamruzzahan, A. S. M.; Wildling, L.; Johnson, W. T.; Ashcroft, B.; Nelson, J.; Lindsay, S. M.; Gruber, H. J.; Hinterdorfer, P. *ChemPhysChem* **2005**, *6*, 897–900.
(40) Stroh, C.; Wang, H.; Bash, R.; Ashcroft, B.; Nelson, J.; Gruber, H.; Lohr, D.; Lindsay, S. M.; Hinterdorfer, P. *Proc. Natl. Acad. Sci. U.S.A.* **2004**, *101*, 12503–12507.
(41) Tang, J.; Ebner, A.; Badelt-Lichtblau, H.; Völlenkle, C.; Rankl, C.; Kraxberger, B.; Leitner, M.; Wildling, L.; Gruber, H. J.; Sleytr, U. B.; Ilk, N.; Hinterdorfer, P. *Nano Lett.* **2008**, *8*, 4312–4319.
(42) Chtcheglova, L. A.; Waschke, J.; Wildling, L.; Drenckhahn, D.; Hinterdorfer, P. *Biophys. J.* **2007**, *93*, L11–L13.
(43) Ebner, A.; Nikova, D.; Lange, T.; Häberle, J.; Falk, S.; Dübbers, A.; Bruns, R.; Hinterdorfer, P.; Oberleithner, H.; Schillers, H. *Nanotechnology* **2008**, *19*, 384017.
(44) Stuart, J. K.; Hlady, V. *Langmuir* **1995**, *11*, 1368–1374.
(45) Hugel, T.; Seitz, M. *Macromol. Rapid Commun.* **2001**, *22*, 989–1016.
(46) Jung, Y. J.; Hong, B. J.; Zhang, W.; Tendler, S. J. B.; Wiliams, P. M.; Allen, S.; Park, J. W. *J. Am. Chem. Soc.* **2007**, *129*, 9349–9355.
(47) Jung, Y. J.; Park, Y. S.; Yoon, K.-J.; Kong, Y.-Y.; Park, J. W.; Nam, H. G. *Nucleic Acids Res.* **2009**, *37*, e10.
(48) Kim, I. H.; Lee, H. Y.; Lee, H. D.; Jung, Y. J.; Tendler, S. J. B.; Williams, P. M.; Allen, S.; Ryu, S. H.; Park, J. W. *Anal. Chem.* **2009**, *81*, 3276–3284.
(49) Clements, J. A. *Mol. Cell. Endocrinol.* **1994**, *99*, C1–6.
(50) Wang, M. C.; Papsidero, L. D.; Kuriyama, M.; Valenzuela, L. A.; Murphy, G. P.; Chu, T. M. *Prostate* **1981**, *2*, 89–96.
(51) Black, M. H.; Giai, M.; Ponzone, R.; Sismondi, P.; Yu, H.; Diamandis, E. P. *Clin. Cancer Res.* **2000**, *6*, 467–473.

{[(tris{[2-carboxyethoxy]methyl}methyl)amino]carbonyl}ethoxy)-methyl]methyl}amino)carbonyl]-2-ethoxy}methyl)methyl]amino}-carbonyl)propylcarbamate (or 27-acid dendron),[47] was purchased from Panagene (www.panagene.com) through custom-order synthesis. The silane coupling agent *N*-(3-(triethoxysilyl)propyl)-*O*-polyethyleneoxide urethane (TPU) was purchased from Gelest Inc. Bis-*N*-succinimidyl(pentaethylene glycol) ester ($BS[PEG]_5$) and dimethyl pimelimidate-2HCl (DMP) were purchased from Pierce. All other chemicals were reagent-grade chemicals from Sigma-Aldrich. All washing solvents for the substrates and the probes were HPLC-grade solvents from Mallinckrodt Laboratory Chemicals. Ultrapure water (18 MΩ·cm) was obtained from a Milli-Q purification system (Millipore). All buffers were freshly prepared and subsequently autoclaved. The antibody 8A6 was obtained from Abcam (UK), and the antibody 5A6 was obtained from Genetex (USA). The PSA was purchased from Calbiochem (USA).

Preparation of AFM Probes. *AFM Probe Pretreatment.* The standard V-shaped silicon nitride probes (MSCT-AUNM, Veeco Instruments; spring constant [ca. 10 pN/nm]) were oxidized by heating in a 10% nitric acid solution at 80 °C for 20 min. The cantilevers were washed and rinsed thoroughly with a copious amount of deionized water. After this cleaning, the cantilevers were dried in a vacuum chamber (30−40 mTorr) for about 20 min and used immediately for the next steps in the process.

Silylation. The above clean probes were placed in 20 mL of anhydrous toluene dissolving 0.20 mL of TPU under nitrogen atmosphere for 4 h. After the silylation, the probes were washed with toluene and baked at 110 °C for 30 min. After the probes were rinsed thoroughly with toluene and then with methanol, they were dried under vacuum (30−40 mTorr).

Preparation of 27-Acid Dendron-Modified Probes. To immobilize the dendron molecule, the above hydroxylated probes were immersed into a methylene chloride solution with a small amount of dimethylformamide (DMF) dissolving 27-acid dendron (1.0 mM) and a coupling agent, 1,3-dicyclohexylcarbodiimide (DCC) (29.7 mM) in the presence of 4-dimethylaminopyridine (DMAP) (0.90 mM) for 12 h. After the coupling reaction, the probes were rinsed thoroughly with methylene chloride, methanol, and water in a sequential manner. Finally, the probes were washed with methanol and dried under vacuum (30−40 mTorr).

Deprotection of 9-Anthrylmethoxycarbonyl Group. The dendron-modified probes were immersed into a methylene chloride solution containing 1.0 M trifluoroacetic acid (TFA) and stirred for 3 h. After the reaction, the probes were soaked in a methylene chloride solution with 20% (v/v) diisopropylethylamine (DIPEA) for 10 min. After the probes were rinsed thoroughly first with methylene chloride and then with methanol, they were kept under vacuum (30−40 mTorr).

Preparing NHS-Modified Probes. The deprotected probes were immersed in an acetonitrile solution containing $BS[PEG]_5$ (25 mM) and DIPEA (1.0 mM) for 4 h under nitrogen. After the reaction, the probes were dipped in a stirred DMF solution for 30 min, washed gently with methanol, and kept under vacuum (30−40 mTorr).

Conjugation of the Detection Antibody to AFM Probes. The activated probes were dipped in a buffer solution (1× PBS [pH 8.5], 0.01% Tween20, and 0.5% glycerol) with the detection antibody (5A6, anti-PSA mouse monoclonal antibody) (0.005 mg/mL) for 2 h and then washed thoroughly with a PBST buffer (PBS with 0.05% Tween20) and a PBS buffer sequentially. After being washed, the probes were stored at 4 °C in a PBS buffer solution (pH 7.4).

Preparation of Immuno Surfaces. *Preparing NHS-Modified Substrates.* The 27-acid dendron-modified slides were activated by immersing in an acetonitrile solution containing di(*N*-succinimidyl)carbonate (DSC) (25 mM) and DIPEA (1.0 mM) for 4 h under nitrogen. After the reaction, they were placed in a stirred DMF solution for 30 min, washed with methanol, and dried under vacuum (30−40 mTorr).

Immobilization of the Capture Antibody on Slides. The capture antibody (8A6, mouse monoclonal anti-PSA) solution (1.0 mg/mL) was prepared with a spotting buffer (1× PBS [pH 8.5], 0.01% Tween20, and 0.5% glycerol), and the antibody was printed on the activated slides using a microarrayer (Cartesian Technologies, Microsys 5100) in a clean room (class 10 000). After the spotting, the printed slides were kept in a humidity chamber (ca. 85% humidity) at room temperature for 3 h. Subsequently, the slides were washed with PBST and deionized water. The washed slides were placed in a blocking solution containing 50 mM ethanolamine in PBS (pH 8.5) for 1.3 h with gentle shaking. Then the slides were washed with PBST and deionized water and dried by spinning them at 1000*g* for 2 min at room temperature.

Sample Incubation and Formation of the Immunocomplex. The solutions of different PSA concentrations in PBS (pH 7.4) were allowed to react with the microspotted antibody at room temperature for 2 h. After the reaction, the slides were washed with a PBST solution and subsequently a PBS solution. For the cross-linking, the slides were treated with a PBS solution (pH 8.5) containing DMP (20 mM) at room temperature for 1 h. Finally, the reaction was quenched by dipping the slides in a Tris solution (20 mM, pH 7.4) for 30 min at room temperature. After washing with a PBST solution, the slides were kept at 4 °C in a PBS solution (pH 7.4) until the analysis (Supporting Information S2).

AFM Force Measurements and Analysis. The AFM measurements were carried out with a NanoWizard AFM (JPK Instrument, Germany) using standard V-shaped silicon nitride probes (MSCT-AUNM, Veeco Instruments; spring constant [ca. 10 pN/nm]). All force measurements were performed in a freshly prepared PBS buffer solution (pH 7.4), and the spring constant of each cantilever was calibrated in solution before each experiment by measuring and analyzing the thermal fluctuation spectrum with NanoWizard software. Different retract velocities ranging from 0.10 to 2.00 μm/s were employed to obtain a set of the measurements. The loading rate was obtained by multiplying the effective spring constant and the retract velocity.

The force−distance curves corresponding to the specific interaction were used for the data analysis. The most probable unbinding force value was determined by fitting the force distribution with the Gaussian curve and taking the mean value. The standard deviation (SD) was estimated by $2\sigma/\sqrt{N}$, where σ is the width of the distribution and N is the number of the rupture events in the histogram.[23]

RESULTS AND DISCUSSION

In a typical protein microarray, antibodies are spotted onto a substrate and are used as probe molecules to capture specific

Scheme 1. Interaction between Captured PSA (Cross-Linked) and Detection Antibody (5A6) during Force Measurement

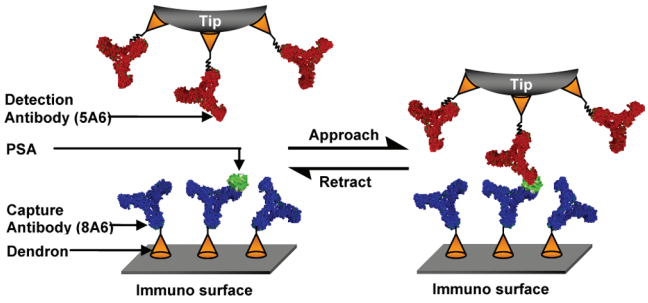

proteins in samples.[52] Herein, we used a pair of monoclonal antibodies, one for capturing the antigens and another for the signal transduction; an antibody (8A6) was immobilized on the 27-acid modified substrate, while another antibody (5A6) was covalently immobilized to an AFM tip that was also modified with 27-acid dendron via a flexible tether attached to the apex of the dendron. Specific PSA binding with the anti-PSA antibody formed an immunocomplex on the surface (Scheme 1). The immunocomplex was chemically cross-linked[53] to avoid a detachment during the force-based detection. Microarray experiments were performed to check the effect of the cross-linking on the interaction between PSA and the detection antibody (5A6). The examination showed that the cross-linking did not induce any significant change (Supporting Information S3), and therefore, assuming no difference in the binding affinity toward 5A6 after the treatment should be a good first approximation. Additionally, the force required to unbind the immunocomplex between PSA and 5A6 was measured independently. The value (55 ± 2 pN) was very close to the one measured after the treatment (Figure 1A).

An immunocomplex composed of 8A6/PSA/5A6 was formed when the AFM tip was in contact with the surface, and a recordable rupture peak was observed when the tip was retracted. Typically, force−distance curves were recorded more than 2 times at each pixel and more than 20 times for those pixels where at least one rupture peak was observed. To map the distribution of the captured PSA, the adhesion force curves were recorded at 3.0 nm intervals across a selected area (120 nm ×120 nm). Appearance of nonlinear stretching was considered as the specific interaction,[48,54] and the distinct hydrodynamic distance corresponding to the immunocomplex helped to differentiate clearly (vide infra).

Figure 1A shows a typical distribution of the specific forces measured at a position where 26 pixels showed specific binding (Figure 2A). The mean value (56 ± 2 pN) is reminiscent of the ones observed from other antigen−antibody pairs.[28,55] To understand the dynamics of the 5A6−PSA interaction, we recorded the unbinding forces at various retraction rates. The mean adhesion force depended on the applied loading rate (Figure 1B). Strict linearity was observed when the most probable unbinding force was plotted against the logarithm of the loading rate. This shows that there is a single energy barrier to go through the rupture process, and the dissociation constant is 2.1×10^{-1} s^{-1}. The kinetic constant is well within the ones reported for other antigen−antibody pairs.[56]

The curves with the characteristic linear adhesion profile were assigned as the ones for the nonspecific events, while the curves with the nonlinear profile were classified as the specific ones (Supporting Information S4). Prior to the antigen−antibody rupture, flexible parts, including the spacers, must be fully stretched; hence, only rupture events with a significant rupture length were categorized as the specific event. A histogram of the unbinding length was obtained from the data, and the Gaussian fit provided a mean value of 13 ± 1 nm (Supporting Information S5).

A force map was generated by putting the mean force value on each pixel. In particular, pixels having a value between 50 and 59 pN were colored with yellow, and pixels with no event cases were represented in black (Figure 2A). For most of the cases, the mean values are within the range, and infrequently, the values below (colored with orange) and above (colored with white) were observed (Supporting Information S6). The linear unbinding profiles coming from nonspecific interactions were collected, and the corresponding pixels were categorized into two groups according to their probability of appearance: a group with less frequency (probability of occurrence ≤ 50%) (red-wine color), and another group with a high frequency (probability of occurrence > 50%) (cyan color).

A single tip was used for scanning at least three different representative positions (center, middle, and outskirts of a microarray spot; ca. diameter = 150 μm). We have observed that a single tip can be used for getting more than 20 000 force curves by adjusting the relative set point so that the maximal compression force is below 300 pN and allowing a certain relaxing time (0.1 s at the largest displacement) at each cycle. It was worthwhile to note that all tips from different batches resulted in consistent numbers of the captured antigens in the area (Supporting Information S7). While there is no fine control for the orientation of the antibodies, it is likely that Fab arms are pointing outward for facile interaction because the constant region rich in lysine reacts with the linker preferentially.[57]

We deliberately started with a smaller pixel for the mapping, and we came up with clusters of pixels that have similar force values and stretching distances. We postulated that the hydrodynamic behavior of the immunocomplex between PSA and 8A6 was associated with the clustering. Upon examination of these well-separated clusters, we found that the diameter of the 12 clusters (from 100 fM PSA) was within 6−10 nm. It would be safe to assume that the hydrodynamic distance is 8 ± 2 nm, and the corresponding circle was used for further analysis. Also, the clustering nature of the immunocomplex helped to unambiguously distinguish the specific sites from the nonspecific sites. We postulated further that the nonspecific sites did not have lateral freedom as much as the immunocomplex had. The distinction

(52) Gul, O.; Calay, E.; Sezerman, U.; Basaga, H.; Gurbuz, Y. *Sens. Actuators, B* **2007**, *125*, 581–588.
(53) Schneider, C.; Newman, R. A.; Sutherland, D. R.; Asser, U.; Greaves, M. F. *J. Biol. Chem.* **1982**, *257*, 10766–10769.
(54) Willemsen, O. H.; Snel, M. M. E.; van der Werf, K. O.; de Grooth, B. G.; Greve, J.; Hinterdorfer, P.; Gruber, H. J.; Schindler, H.; van Kooyk, Y.; Figdor, C. G. *Biophys. J.* **1998**, *75*, 2220–2228.
(55) Dammer, U.; Hegner, M.; Anselmetti, D.; Wagner, P.; Dreier, M.; Huber, W.; Güntherodt, H.-J. *Biophys. J.* **1996**, *70*, 2437–2441.
(56) Schwesinger, F.; Ros, R.; Strunz, T.; Anselmetti, D.; Güntherodt, H.-J.; Honegger, A.; Jermutus, L.; Tiefenauer, L.; Plückthun, A. *Proc. Natl. Acad. Sci. U.S.A.* **2000**, *97*, 9972–9977.
(57) Idiris, A.; Kidoaki, S.; Usui, K.; Maki, T.; Suzuki, H.; Ito, M.; Aoki, M.; Hayashizaki, Y.; Matsuda, T. *Biomacromolecules* **2005**, *6*, 2776–2784.

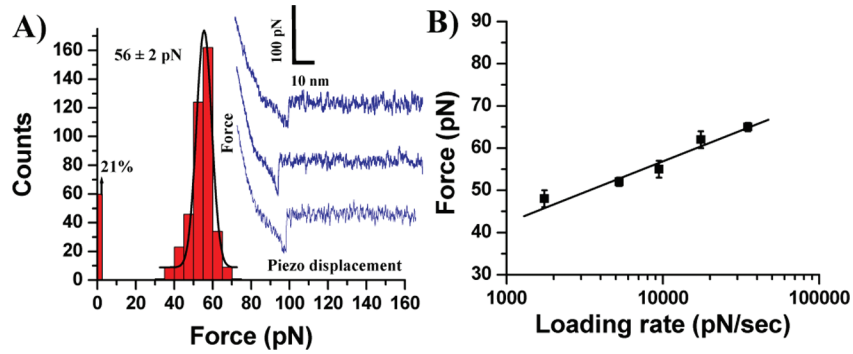

Figure 1. Histogram of adhesion forces recorded for specific interaction between PSA and the detection antibody and dynamics of the interactions. (A) Corresponding unbinding force histogram (mean ± SD, $n = 603$) together with the representative force−distance curves; the % value next to the *y* axis represents the percentage of no event. (B) Loading rate dependence of the unbinding forces for antibody−immunocomplex interaction. At each loading rate, more than 100 data were recorded.

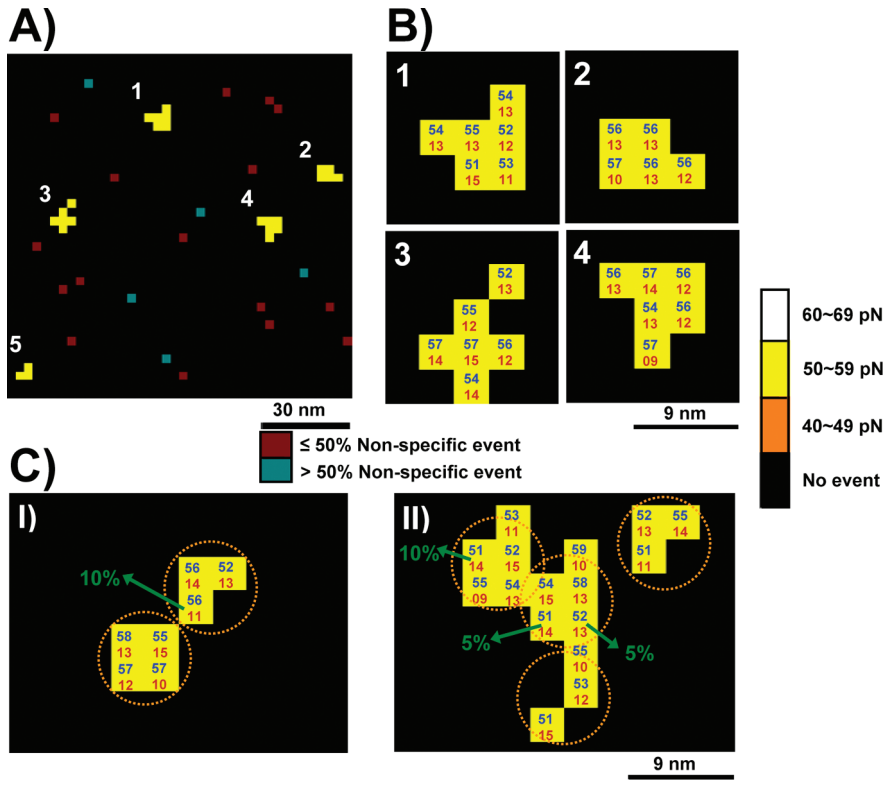

Figure 2. Spatially resolved maps obtained from the interaction between PSA and detection antibody. (A) One of the adhesion force maps recorded at 100 fM PSA. (B) Four clusters out of 12 observed at 100 fM (magnified images); more than 20 force curves were recorded at each specific pixel; the number in blue represents the mean force value in pN, and the one in red is the mean stretching distance in nm (the percentage of the specific event at each pixel is presented in Supporting Information S13). (C) Two representative clusters showing the double peaks: (I) the double peak shows at only the adjacent pixels; (II) the double peaks show not only at the adjacent pixels but also at the pixels away from the overlapping area. The % values represent the percentage of double peaks out of the total measured curves corresponding to each pixel.

was another valuable criterion when the specific sites were unambiguously discriminated from the nonspecific ones.

A close look at the clusters provided additional information. Typical clusters (Figure 2B) showed uniform mean force values (51−57 pN) and stretching distance values (9−15 nm). At higher concentrations of PSA, some clusters were close (Figure 2C). It was interesting to observe double rupture peaks in these particular cases, as we observed only single rupture curves at other separate clusters. The pixels showing the double peaks are indicated by an arrow with the percentage of getting the double peak. In most of the cases, the double peaks were observed at the boundary sections (case I), but there are some cases where nonadjacent pixels showed the double peaks (case II). These phenomena could be interpreted with possible models shown in Scheme 2. It is possible that one 5A6 can form a complex with two captured antigens when they are in proximity (case A). The span of 5A6 is long enough to show the double peaks at the nonadjacent pixels. Alternatively, the two Fab arms of two different 5A6 come into play with the antigens (case B). It is less likely that two PSAs are bound at a single 8A6 at such concentrations (case C). Observations indicate that mapping at the nanoscale resolution is particularly helpful when the antibody−antigen interaction is studied with

Scheme 2. Schemes of Possible Configurations Giving Rise to Double Peaks

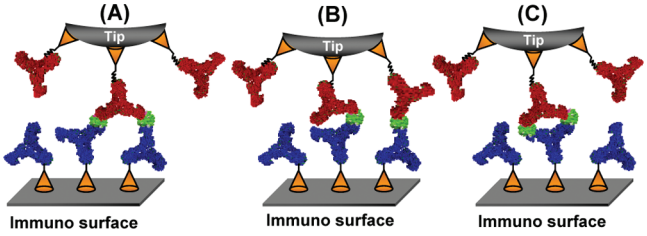

force-based AFM because more information regarding the source of the multiple peaks can be obtained.

"Seeing and counting" the captured antigens in a quantitative manner would be beneficial for understanding the equilibrium on a microarray. A single cluster was observed within the total scanned area (3 × 120 nm × 120 nm) with 10 fM of PSA. With higher concentrations, such as 100 fM, 1.0 pM, and 10 pM, the number was 12 (= 3 + 5 + 4), 54 (= 21 + 14 + 19), and 76 (= 25 + 28 + 23) clusters, respectively (Supporting Information S6). Approximately 82% of antigens in the sample solution of 100 fM were bound to the microarrayed spot (Supporting Information S8). While 10 fM is the detection limit with the current format (a spot of 150 μm), it is expected that the limit can be lower as long as the spot size is reduced. Also, a wide dynamic range can be achieved when a combination of spots of various sizes is used.

Since atomic force microscopes suffer from the inherent drift to a certain degree, it is necessary to be cautious in obtaining and interpreting the force images. For example, the currently employed assay relies on mapping the clusters of which shape is a function of the hydrodynamic distance and the pixel size. In order to avoid the distortion of clusters in terms of shape and total size, the lateral drift, in particular during the scanning of a few lines, should be minimal. It is desirable to correct it by using a suitable drift compensation method if necessary. Employing high retraction speed to reduce the scan time or applying a newly developed approach like TREC is an alternative solution. The short assay time is an additional advantage of such approach as long as the specificity and the reproducibility can be maintained.

Several control experiments were performed for further confirmation. We scanned the surface without exposing it to PSA and confirmed absence of the cluster corresponding to the captured PSA. Also, a solution of 5A6 (0.01 mg/mL) was allowed to block the immunocomplex formed by PSA and the capture antibody. The scanning showed only pixels with nonspecific binding (Supporting Information S9). Moreover, the capture antibody surface was incubated with a high concentration of PSA (1.0 μM), and then the surface was examined. Sixteen clusters corresponding to the immunocomplex were observed within the scanned area (60 nm × 60 nm) (Supporting Information S10). As the first approximation, the surface density of the clusters ($4.4 \times 10^3/\mu m^2$) can be regarded as the lower limit value of the capture antibody. Furthermore, the same surface was examined in the presence of free PSA (0.5 μM) to block the detection antibodies during the measurement. As expected, the adhesion map (Supporting Information S11) showed that the pixels for the specific interaction had almost disappeared. Only a few pixels showed the specific interaction, and insufficient blocking at this condition may explain the only remaining cluster on the map.

To investigate an effect of nontarget analytes, the same experiment was performed (Supporting Information S12) in a mixture of interfering substances (triglycerides, 250 mg/dL; transferring, 5.0 mg/mL) and human serum albumin (1.0 mg/mL). There was no significant change in total numbers of the antigens counted within the total scanned area.

CONCLUSIONS

In this study, we observed that the dendron modification of the tip and the substrate enabled the force-based AFM to "see and count" individual antigens captured on an antibody microarray, and the nanoscale maps showed the hydrodynamic behavior of the immunocomplex. Also, our results indicate that the approach can be applicable to the quantitative analysis of the antigen in a sample and imply that it can be extended to a sample of very low copy numbers as long as the size of the microarrayed spot is reduced. Also, the maps indicate that addressing the individual immunocomplex helps to understand the behavior of the complex during the force measurement. We believe that the approach can be extended to other protein biomarkers and could provide AFM with a new function for ultrasensitive immunodetection.

ACKNOWLEDGMENT

J.W.P. acknowledges financial support from an NCRC Grant funded by the Korean government (MEST) (2009-0091507), the Nano/Bio Science & Technology Program of MEST (2005-01325), a R&D Program for Fusion Strategy of Advanced Technologies (MKE), and the Brain Korea 21 program.

SUPPORTING INFORMATION AVAILABLE

Chemical structure of 27-acid dendron, schematic diagram for the surface treatment, microarray data, representative force−distance curves, unbinding length distribution, calculation of the bound antigen, and adhesion maps obtained from various conditions. This material is available free of charge via the Internet at http://pubs.acs.org.

Received for review February 22, 2010. Accepted April 28, 2010.

AC100476B